Pergamon

PII: S0191-8141(97)00067-9

Journal of Structural Geology, Vol. 19, No. 12, pp. 1521 to 1526, 1997

0191-8141/97 $17.00 + 0.00

Static recovery and recrystallization microstructures in sheared octachloropropane

J.-H. REE

Department of Earth and Environmental Sciences, Korea University, Anam-dong, Seongbuk-ku, Seoul 136-701, Korea

and

Y. PARK*

Department of Geological Sciences, University at Albany, Albany, NY 12222, U.S.A.

(*Received* 31 *May* 1996; *accepted in revised form* 4 *August* 1997)

Abstract—Octachloropropane (C_3Cl_8) was sheared using a press mounted on an optical microscope and then allowed to adjust its microstructure statically, at the deformation temperature. Depending on strain rate and deformation temperature, the post-deformational changes in microstructure are strikingly different. After low temperature–high strain-rate deformation, fast growth of new strain-free grains on the boundaries of deformed grains results in the obliteration of grain-shape foliation and intracrystalline deformation features, and the development of a foam texture. After high temperature–low strain-rate deformation, on the other hand, grain-shape foliation and grains with subgrain boundaries tend to survive the adjustment. Lattice preferred orientation is maintained after the post-deformational adjustment at both deformation conditions and thus remains a good indicator of deformation. © 1997 Elsevier Science Ltd.

INTRODUCTION

During the last two decades geologists have used microstructures of deformed rocks extensively to infer deformation processes, mechanisms and conditions, usually assuming that there is almost no change in microstructure when deformation stops. However, it is widely recognized that post-deformational changes in microstructures can occur at the end of an orogeny when deformation has essentially ceased and the rocks are at high temperatures (> 300°C) or when deformed rocks are subjected to sustained heating from post-tectonic plutons (e.g. Green *et al.*, 1970; Urai *et al.*, 1986; Knipe, 1989; Passchier and Trouw, 1996, pp. 45–47). In these cases, care must be taken in interpreting microstructures as the effects of post-deformational changes are unknown. Experiments evaluating textural changes due to static heating after deformation are limited: on quartz aggregates by Green (1967), Green *et al.* (1970), Ralser (1987) and Gleason and Tullis (1990); on calcite aggregates by Griggs *et al.* (1960); on olivine aggregates by Karato (1989); on camphor by Urai and Humphreys (1981); and on octachloropropane by Means and Dong (in press).

In this paper we report further results on octachloropropane and show that the effects of post-deformational adjustment of microstructures are strikingly different depending on the deformation conditions (i.e. high strain rate–low temperature or low strain rate–high temperature). Under both conditions, octachloropropane aggregates show extensive recrystallization during deformation, but static recrystallization after deformation is much more pronounced in samples deformed at high strain rate and low temperature. This kind of post-deformational recrystallization after 'hot working' has been called 'metadynamic recrystallization' by metallurgists (Djaic and Jonas, 1972).

EXPERIMENTAL METHOD

The experimental material was octachloropropane (C_3Cl_8, hereafter called OCP) mixed with marker particles (1000-grit silicon carbide). The optical properties of OCP and techniques of sample preparation are given by Jessell (1986), Means and Ree (1988) and Ree (1991, 1994a). We used OCP purified at the Utrecht University for deformation experiments using computer-aided synkinematic microscopy (Means, 1989). The details of this method (microstructural analysis in synkinematic microscopy using NIH image) are explained by Park (1996).

Samples were deformed under simple shearing or general shearing flow. One group of experiments was conducted at lower temperatures (18–20°C, or 67–68% of the absolute melting temperature of OCP) and higher strain rates (10^{-1}–10^{-4} s^{-1}). The second group was done at higher temperatures (70–80°C, or 79–82% of the absolute melting temperature) and lower strain rate (10^{-5} s^{-1}). After deformation the samples were left in the press and the deformation temperature was maintained for from 47 min to 40 h 19 min for low

* Present address: Department of Earth and Environmental Sciences, Korea University, Anam-dong, Seongbuk-ku, Seoul 136-701, Korea.

temperature–high strain-rate experiments, and from 4 h 31 min to 56 h 40 min for high temperature–low strain-rate experiments. We then measured the orientation of the *c*-axes on a universal stage.

A total of 26 low temperature–high strain-rate and eight high temperature–low strain-rate experiments were conducted. In the following section we describe the experimental results of two representative samples from each group.

CD ROM and video tape

Time-lapse movies of experiments including the ones not described in this paper were stored on video tape and CD ROM. The video tape and CD ROM can be provided by the authors at a nominal cost including mailing charge.

EXPERIMENTAL RESULTS

Low temperature–high strain-rate experiment (TO-334)

The sample before deformation showed a foam texture of optically strain-free equiaxed grains, a few with straight subgrain boundaries inside them (Fig. 1a). Lattice preferred orientation (LPO) always develops during sample preparation when samples are pressed perpendicular to the plane of observation to produce an appropriate sample thickness (30–40 μm, producing a gray to yellow interference color of OCP crystals) and OCP extrudes parallel to the grips on the glass slides (parallel to the future shearing direction) (see Fig. 3a).

The deformation geometry of the experiment is a general shearing type in which there is some extension parallel to the shearing direction and some shortening perpendicular to it. The pattern of marker particle trajectories (not shown) is consistent with this deformation geometry. The sample was deformed at low temperature (20°C) and high strain rate ($10^{-3.5}$ s^{-1}). A total shear strain of about 0.8 was imposed over 38 min and then the deformation temperature was maintained for 22 h 53 min without deformation.

With the initiation of deformation, grain boundaries become serrated and begin to migrate. Undulose extinction and deformation bands develop inside the grains, suggesting intracrystalline plastic deformation (Fig. 1b–d). New subgrain boundaries appear within some grains. A grain-shape foliation begins to develop oblique to the shear direction at a bulk shear strain of 0.2 (Fig. 1b). With further deformation, the intensity of the grain-shape foliation increases while its orientation remains in more or less the same orientation. During the deformation, some grains nucleate and grow fast on the boundaries of old grains. However, the majority of grains at the end of deformation are the same ones present before deformation. In Fig. 1(d), 84% of the field of view (in area) is occupied by the grains present at the beginning of deformation. Also, there is no significant change in average grain size during the deformation.

The period after the press motor was turned off was not entirely static because there were slight displacements of marker particles during the nominally static interval, resulting in an additional shear strain of less than 0.02 which was probably caused by relaxation of elastic strains in the loading system. After deformation, new strain-free grains grow rapidly on the grain boundaries and totally destroy deformation microstructures such as grain-shape foliation and intracrystalline deformation features of old grains, resulting in a foam texture (Fig. 1e–h). This rapid growth of new grains takes place for about 1.5 h after deformation. After this period, slow, normal grain growth (Smith, 1964) takes over, presumably via grain-boundary-energy-driven grain boundary migration (Bons and Urai, 1992). The final microstructure after post-deformational change (Fig. 1h) looks much like that of the undeformed material (Fig. 1a), except that there has been an increase in average grain size in Fig. 1(h). New recrystallized grains which nucleated and grew on the boundaries of the initial grains in Fig. 1(d), occupy about 60% of the total area in Fig. 1(h). Some of the grains originated from subgrains along the margin of the deformed grains. Note also that many of the 'old' grains in Fig. 1(h) tend to be small compared to 'new' grains, and it is expected that these smaller old grains will disappear via further normal grain growth.

The *c*-axes could not be measured immediately after deformation because of the fast growth of new grains. By stage h of Fig. 1 the sample shows a strong LPO with the *c*-axis fabric forming a single girdle approximately perpendicular to the shear zone boundary (Fig. 3b). Image recordings with the gypsum plate inserted (not shown) confirmed that the *c*-axis fabric immediately after deformation is similar to that after post-deformational heating. This is also supported by plotting *c*-axes of new and old grains separately at the stage of Fig. 1(h) (Fig. 4). It can be seen that the *c*-axis fabric of new grains is very similar to that of old grains.

High temperature–low strain-rate experiment (TO-312)

Sample TO-312 was deformed under the same general shearing geometry as TO-334. A total shear strain of about 0.5 was imposed over 5 h 50 min at high temperature (80°C) and low strain rate ($10^{-4.7}$ s^{-1}). Then the deformation temperature was maintained for 56 h 40 min without further deformation. As the sample deforms, grain boundaries begin to migrate. In contrast to low temperature–high strain-rate deformation, the migrating grain boundaries are not serrated. Instead they are straight or slightly wavy in most cases, and lobate in some cases (Fig. 2b & c). Undulose extinction and deformation bands are common within the grains. Subgrain boundaries are well developed, generally at high angles ($\sim$90°) to shear zone boundaries and parallel

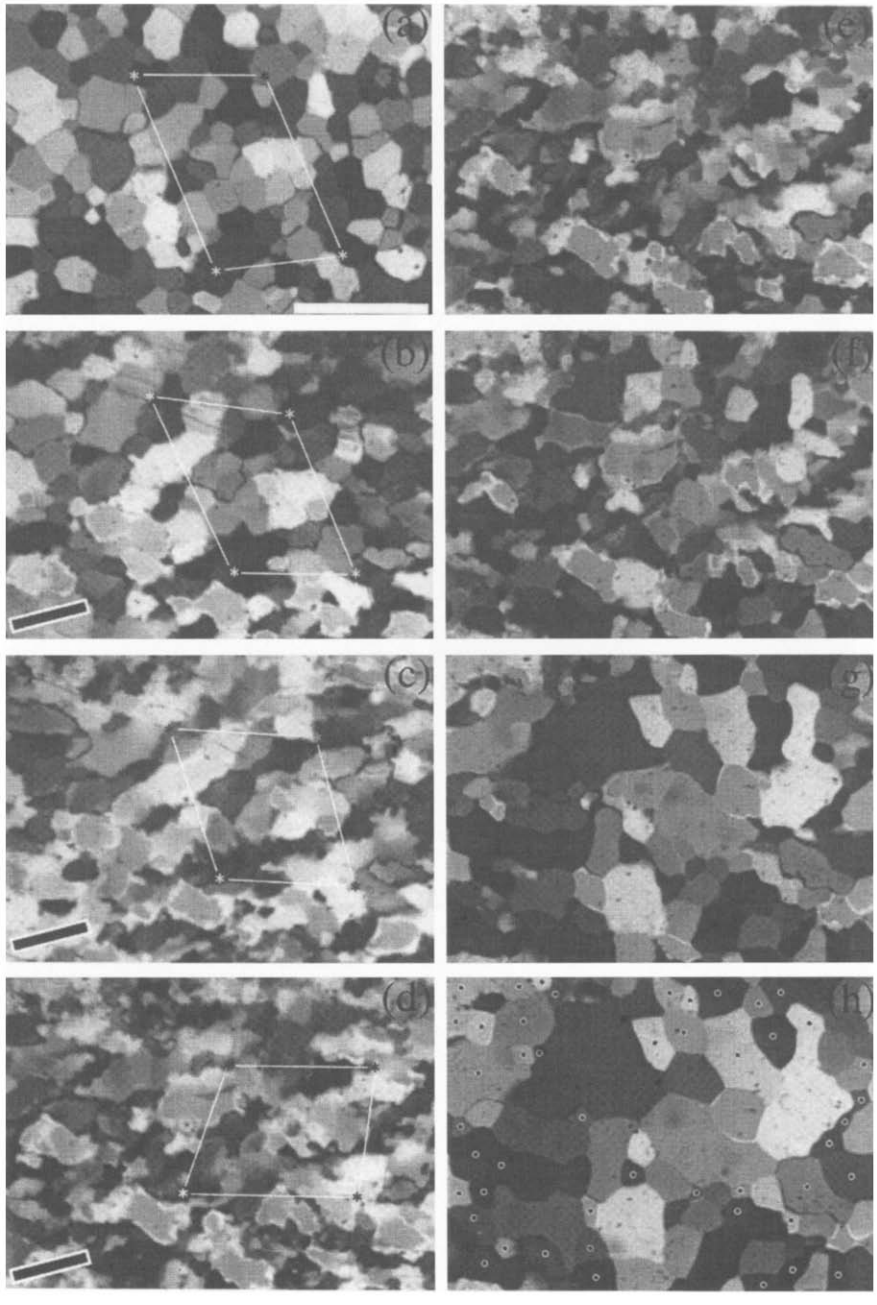

Fig. 1. Photomicrographs of sample TO-334 deformed at low temperature (20°C)–high strain rate ($10^{-3.5}$ s^{-1}). (a) Before deformation; (b) & (c) during deformation; (d) at the end of deformation with bulk $\gamma = 0.8$; (e)–(h) during static heating after deformation. Times after deformation as follows: (e) 19 min; (f) 49 min; (g) 2 h 11 min; and (h) 22 h 53 min. Duration of deformation is 38 min. The shear zone boundary is parallel to the length of the photographs. Asterisks represent selected marker particles. Solid bar in (b)–(d) indicates the orientation of the grain-shape foliation. Grains with a black dot in (h) are old ones which were initially present in (d). Cross-polarized light. Scale bar in (a) is 0.5 mm.

to the *c*-axes of the grains (Fig. 2c). The development of subgrain boundaries is a major difference from samples deformed at low temperature and high strain rate. A detailed account of subgrain boundary development at high temperature and low strain rate is given by Means and Ree (1988) and Ree (1994b). Although some subgrain boundaries become grain boundaries with increasing misorientation, no new grains nucleate and grow on the grain boundaries. The grain size increases, mainly by grain boundary migration and 'amalgamation' (Means, 1989) during deformation. The deformation processes of OCP at these conditions are described in detail by Means and Ree (1988) and Ree (1990, 1991, 1994a,b).

During post-deformational adjustment smaller grains tend to disappear (Fig. 2d–f). Also a multiplication of subgrain boundaries (type VII subgrain boundary of Means and Ree, 1988) appears in some grains, which occurs statically from optically strain-free grains by a process probably similar to classical poligonization. However, there is not much change in the optical microstructure during post-deformational adjustment

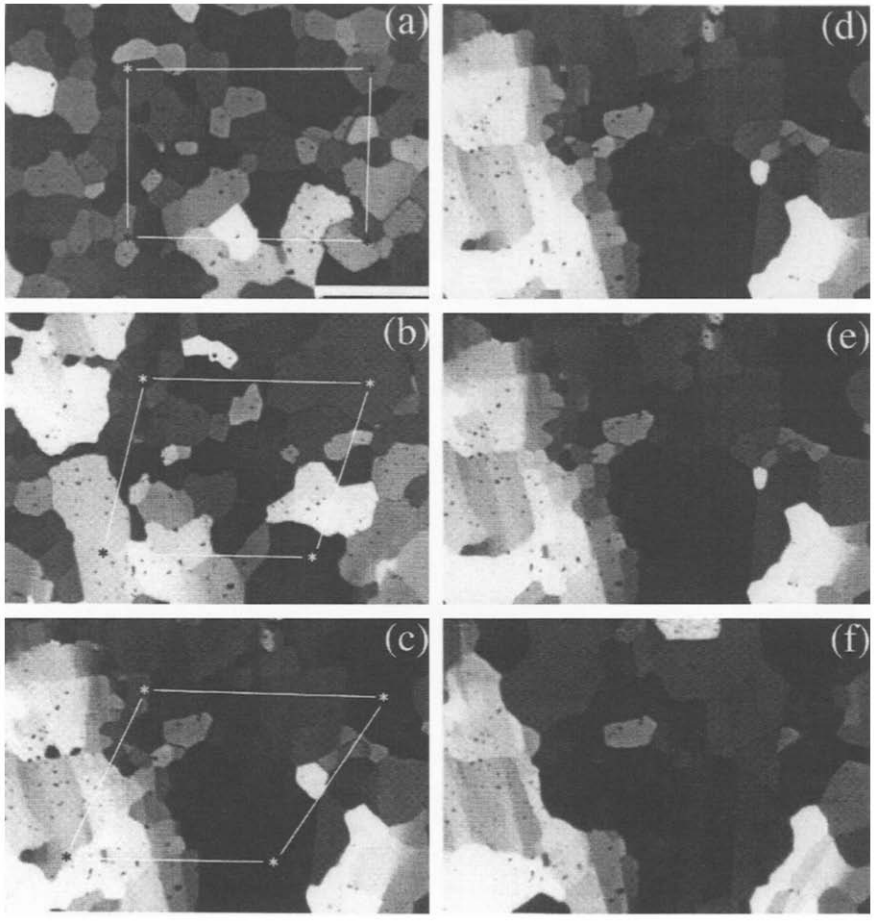

Fig. 2. Photomicrographs of sample TO-312 deformed at high temperature (80°C)–low strain rate ($10^{-4.7}$ s^{-1}). (a) Before deformation; (b) during deformation; (c) at the end of deformation with $\gamma = 0.5$; (d)–(f) during static heating after deformation. Times after deformation as follows: (d) 10 h 42 min; (e) 23 h 12 min; (f) 56 h 40 min. Duration of deformation is 5 h 50 min. The shear zone boundary is parallel to the length of the photographs. Asterisks represent selected marker particles. Cross-polarized light. Scale bar in (a) is 0.25 mm.

(Fig. 2d–f). The *c*-axis fabric after post-deformational adjustment shows a strong LPO which forms a point-maximum approximately perpendicular to the shear-zone boundary (Fig. 3c). This LPO is certainly inherited from that occurring immediately after deformation because most of the grains survive the post-deformational heating.

DISCUSSION

Our observations indicate that OCP deforms mainly by dislocation creep under both low temperature–high strain-rate and high temperature–low strain-rate conditions. However, the dynamic recovery mechanism (recovery *during* deformation) is different in each regime. At low temperature–high strain rate, recrystallization by grain boundary migration is the dominant recovery mechanism. At high temperature–low strain rate, on the other hand, both dislocation climb (evidenced by extensive development of subgrain boundaries) and recrystallization by grain boundary migration are the dominant recovery mechanisms. Similar results have been reported in experimentally deformed quartz aggregates by Hirth and Tullis (1992).

In the sample deformed at low temperature–high strain rate, new grains nucleate and grow fast on the boundaries of deformed grains during post-deformational adjustment, probably driven by stored strain energy. Then normal grain growth driven by surface energy (Smith, 1964) occurs slowly. These processes totally erase former deformation microstructures. However, static recrystallization during post-deformational adjustment does not significantly alter the LPO, even though many of the grains present are recrystallized ones. The preservation of LPO is probably due to the host control on lattice orientation of newly recrystallized grains (Hobbs, 1968; Urai *et al.*, 1986). This suggests a possibility that apparently undeformed rocks with LPO may have experienced a previous deformation and then post-deformational static recrystallization, although these rocks would usually bear other deformation indicators such as fold, foliation and/or lineation defined by preferred orientation of other mineral phases.

The sample deformed at high temperature–low strain rate does not experience much change in microstructure

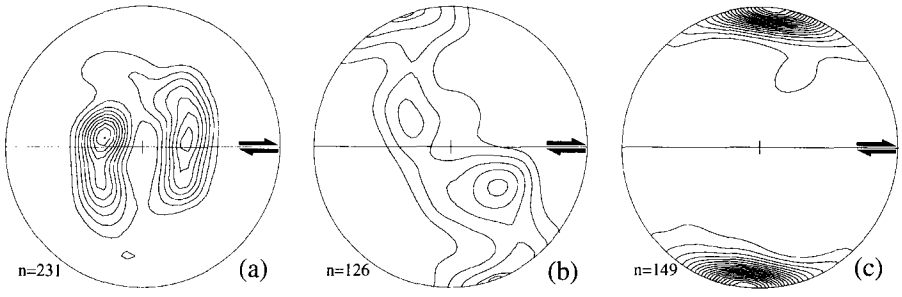

Fig. 3. c-axis fabric diagrams. (a) Typical c-axis pattern of the OCP sample before deformation. (b) Sample TO-334 at $t = 22$ h 53 min after deformation. (c) Sample TO-312 at $t = 23$ h 12 min after deformation. Lower-hemisphere, equal-area projections. The contor interval is 2σ (σ = standard deviation).

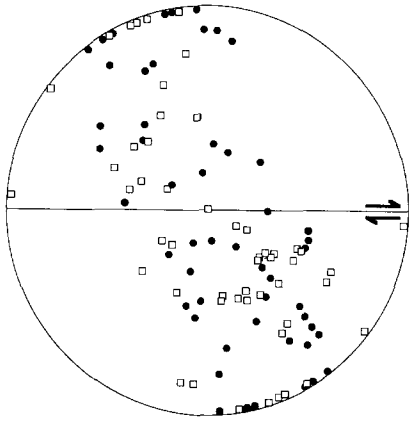

Fig. 4. c-axis plot of new (open square) and old (solid circle) grains at stage of Fig. 1(h) in sample TO-334. Lower-hemisphere, equal-area projection.

during post-deformational adjustment. The only changes that can be recognized are the disappearance of a few smaller grains due to grain growth driven by surface energy and development of type VII subgrain boundaries (Means and Ree, 1988) in some grains. As a result, the LPO reflects that immediately after deformation. The preservation of microstructures indicates that the sample has already reached a low strain-energy (thus stable) configuration at the end of deformation, with the development of subgrain boundaries by dislocation climb. Also, the rate of grain growth after deformation is much slower than that in the low temperature–high strain-rate experiment probably due to the initially larger grain size at the end of deformation. Although the sample deformed at high temperature–low strain rate in this paper develops too weak a foliation to describe, Ree (1991) has shown that once grain-shape foliation develops under this condition its orientation and intensity can survive the post-deformational adjustment (see fig. 2h of Ree, 1991). Also Ree (1994b) has described how the mean orientation of subgrain boundaries and the subgrain-boundary density (the total length of subgrain boundaries divided by the observation area) do not change much through a static adjustment after deformation at these conditions.

It is not clear why the LPO pattern of the sample deformed at low temperature–high strain rate (single girdle) is different from that at high temperature–low strain rate (point maximum). The point maximum of TO-312 may be due to the development of 'ribbon' grains, in which the basal slip planes are parallel to the shear zone boundary, at high strain-rate zones near both grips (thus near the shear zone boundaries; ribbon grains are not in the field of view of Fig. 2). The displacement jump toward the shear zone boundaries has been confirmed by the analysis of marker particle trajectories of TO-312. Alternatively, the single girdle of TO-334 may result from the operation of prism $<a>$ slip in addition to basal $<a>$ slip as the dominant slip system switches from basal $<a>$ slip to prism $<a>$ slip with increasing strain rate in OCP (Jessell, personal communication, 1989).

Although our experiments showed two contrasting microstructural developments, it is not clear whether the results from this material can be applied to the interpretation of natural microstructures. If similar processes operate in naturally deformed rocks, our results may have important implications for deciphering natural microstructures, especially when deformed rocks have been subjected to a prolonged period of high temperature after deformation.

CONCLUSIONS

(1) After low temperature–high strain-rate deformation many of the deformed grains disappear and new strain-free grains grow on the boundaries of the deformed grains to establish a foam texture. After high temperature–low strain-rate deformation, on the other hand, most of the deformed grains tend to survive.

(2) Grain-shape foliation is totally destroyed with the development of foam texture after low temperature–high strain-rate deformation. Grain-shape foliation can remain after high temperature–low strain-rate deformation.

(3) Subgrain boundaries developed during high temperature–low strain-rate deformation are stable throughout the post-deformational adjustment.

(4) LPO provides a more durable record of deformation than oblique foliation in OCP. Recrystallization after low temperature–high strain-rate deformation destroys the latter.

Acknowledgements—This experimental work was done during J.-H. Ree's research visit and Y. Park's post-doctoral research at the University at Albany. J.-H. Ree thanks W. D. Means for his kind invitation. We appreciate comments on an earlier version of the manuscript by W. D. Means, J. Tullis, M. Herwegh and J. L. Urai. We also thank J. P. Evans and two anonymous referees for their constructive and helpful reviews. This research was supported by KOSEF grant 941-0400-003-2 to J.-H. Ree and NSF grant EAR-9404872 to W. D. Means. The Center for Mineral Resources Research at Korea University provided additional funds for the research visit of J.-H. Ree.

REFERENCES

Bons, P. D. and Urai, J. L. (1992) Syndeformational grain growth: microstructures and kinetics. *Journal of Structural Geology* **14**, 1101–1109.

Djaic, R. A. P. and Jonas, J. J. (1972) Static recrystallization of austenite between intervals of hot working. *Journal of the Iron and Steel Institute* **210**, 256–261.

Gleason, G. C. and Tullis, J. (1990) The effect of annealing on the lattice preferred orientations of deformed quartz aggregates. *EOS, Transactions of the American Geophysical Union* **71**, 1657.

Green, H. W. (1967) Quartz: extreme preferred orientation produced by annealing. *Science* **157**, 1444–1447.

Green, H. W., Griggs, D. T. and Christie, J. M. (1970) Syntectonic and annealing recrystallization of fine-grained quartz aggregates. In *Experimental and Natural Rock Deformation*, ed. P. Paulitsch, pp. 272–335. Springer, New York.

Griggs, D. T., Paterson, M. S., Heard, H. C. and Turner, F. J. (1960) Annealing recrystallization in calcite crystals and aggregates. In *Rock Deformation*, eds D. T. Griggs and J. Handin, pp. 21–37. Memoir of the Geological Society of America **79**.

Hirth, G. and Tullis, J. (1992) Dislocation creep regimes in quartz aggregates. *Journal of Structural Geology* **14**, 145–159.

Hobbs, B. E. (1968) Recrystallization of single crystals of quartz. *Tectonophysics* **6**, 353–401.

Jessell, M. W. (1986) Grain boundary migration and fabric development in experimentally deformed octachloropropane. *Journal of Structural Geology* **8**, 527–542.

Karato, S. (1989) Grain growth kinetics in olivine aggregates. *Tectonophysics* **168**, 255–273.

Knipe, R. J. (1989) Deformation mechanisms—recognition from natural tectonites. *Journal of Structural Geology* **11**, 127–146.

Means, W. D. (1989) Synkinematic microscopy of transparent polycrystals. *Journal of Structural Geology* **11**, 163–174.

Means, W. D. and Dong, H. (in press) Post-deformational recovery of microstructure in sheared octachloropropane (C_3Cl_8). In *Fault-related Rocks—A Photographic Atlas*, eds A. W. Snoke, J. Tullis and V. R. Todd. Princeton University Press, Princeton.

Means, W. D. and Ree, J.-H. (1988) Seven types of subgrain boundaries in octachloropropane. *Journal of Structural Geology* **10**, 765–770.

Park, Y. (1996) Synkinematic microscopic analysis using NIH Image. In *Structural Geology and Personal Computers*, ed. D. De Paor, pp. 123–134. Pergamon, Oxford.

Passchier, C. W. and Trouw, R. A. J. (1996) *Microtectonics*. Springer, Berlin.

Ralser, S. (1987) Experimental deformation of a quartz mylonite. Ph.D. thesis, University of Monash.

Ree, J.-H. (1990) High temperature deformation of octachloropropane: dynamic grain growth and lattice reorientation. In *Deformation Mechanisms, Rheology and Tectonics*, eds R. J. Knipe and E. H. Rutter, pp. 363–368. Geological Society of London Special Publication **54**.

Ree, J.-H. (1991) An experimental steady-state foliation. *Journal of Structural Geology* **13**, 1001–1011.

Ree, J.-H. (1994a) Grain boundary sliding and development of grain boundary openings in experimentally deformed octachloropropane. *Journal of Structural Geology* **16**, 403–418.

Ree, J.-H. (1994b) Subgrain boundaries in octachloropropane: deformation patterns, subgrain boundary orientation and density. *Journal of the Petrological Society of Korea* **3**, 20–33.

Smith, C. S. (1964) Some elementary principles of polycrystalline microstructure. *Metallurgical Reviews* **9**, 1–48.

Urai, J. L. and Humphreys, F. J. (1981) The development of shear zones in polycrystalline camphor. *Tectonophysics* **78**, 677–685.

Urai, J. L., Means, W. D. and Lister, G. S. (1986) Dynamic recrystallization of minerals. In *Mineral and Rock Deformation: Laboratory Studies—The Paterson Volume*, eds H. C. Heard and B. E. Hobbs, pp. 161–199. American Geophysical Union Geophysical Monograph **36**.